RSC Advances

PAPER

View Article Online
View Journal | View Issue

Open Access Article. Published on 13 February 2025. Downloaded on 1/20/2026 2:38:44 PM.
This article is licensed under a Creative Commons Attribution-NonCommercial 3.0 Unported Licence.

Check for updates

Cite this: *RSC Adv.*, 2025, **15**, 4904

Annona squamosa seeds capped calcium oxide nano particles – anti-microbial, antioxidant, anti-ulcer analysis

Sarathamani T,[a] Kalaiselvi V,*[a] Blessymol B,[a] Gopi S,[b] Gulrana Khuwaja,[c] Sivasubramanian Palanismy,*[d] Khatib Sayeed Ismail,[e] Syed Kashif Ali,[fg] Mika Sillanpaa[hijklm] and Nadir Ayrilmis*[n]

Received 15th January 2025
Accepted 1st February 2025

DOI: 10.1039/d5ra00375j

rsc.li/rsc-advances

Calcium Oxide (CaO) is the best replica of logically plentiful earth metal oxides. CaO nanoparticles include sphere-shaped or faceted elevated surface area and magnetic nanostructured particles. The current study give the information regarding booming synthesis of calcium oxide nanoparticles using calcium chloride as precursor and *Annona squamosa* seed extract as capping agent. The main goal of using a biological approach to synthesize CaO NPs is to reduce the use of dangerous chemicals in the process, which will be more economical and environmentally friendly. This is the initial time seeds have been utilised for green nanoparticle deposition. The synthesized powder was golden yellow colour. The obtained CaO NPs have been characterized by X-ray diffraction, scanning electron microscope, ultra violet visible spectroscopy, Fourier transform infra-red, dynamic light scattering studies. The synthesized samples are applied for phytochemical screening, anti-bacterial, anti-fungal, antioxidant and anti-ulcer applications.

1. Introduction

Nanotechnology involves the relevance of scientific principles to operate matter at the molecular level.[1] Remarkable advancements in this field have enabled innovations such as nano-biotechnology, bio-nanotechnology, quantum dots, and surface-enhanced Raman scattering (SERS), leading to unique, straightforward, and practical breakthroughs in materials science and engineering.[2] The main goals of using a green synthetic technique are to synthesize a range of metals and metal oxides while minimizing the use of hazardous chemicals, preventing waste, being efficient, being inexpensive, and producing products with a relatively high yield. Magnesium oxide (MgO), titanium oxide (TiO_2), copper oxide (CuO), zinc oxide (ZnO), and calcium oxide (CaO) are the most common inorganic nano metal oxides. These stable, antimicrobial, and multifunctional nano metal oxides pose no threat to humans or other living things.[3,4] The utilisation of bio extracts in the production of nanoparticles has been proven to be a financially viable approach that expands the scope of non-toxic nanoparticle synthesis. Oxide of calcium (CaO) applications for nanoparticles include water filtration, adsorption, catalysis, and antibacterial agents. Calcium oxide nanoparticles are employed as feasible drug delivery agents in photothermal and photodynamic therapy as well as synaptic administration because of their unique structural and optical characteristics.[5] The *Annona squamosa* shrub or tree, belonging to the Annonaceae family, has sugar apple-flavored fruits. Around the world, sugar apples are grown on tropical plains in regions including Africa,

[a]Department of Physics, Navarasam Arts and Science College for Women, Arachalur, Erode-638101, Tamil Nadu, India. E-mail: nk.arthi.kalai@gmail.com
[b]Department of Physics, Sri Ramakrishna Mission Vidyalaya College of Arts and Science, Coimbatore-20, Tamil Nadu, India
[c]Department of Pharmaceutical Chemistry and Pharmacognosy, College of Pharmacy, Jazan University, Jazan 45142, Kingdom of Saudi Arabia
[d]Department of Mechanical Engineering, PTR College of Engineering and Technology, Austinpatti, Madurai – Tirumangalam Road, Madurai – 625008, Tamil Nadu, India. E-mail: sivaresearch948@gmail.com
[e]Department of Biology, College of Science, Jazan University, P.O. Box. 114, Jazan 45142, Kingdom of Saudi Arabia
[f]Department of Physical Sciences, Chemistry Division, College of Science, Jazan University, P.O. Box. 114, Jazan 45142, Kingdom of Saudi Arabia
[g]Nanotechnology Research Unit, College of Science, Jazan University, P.O. Box. 114, Jazan 45142, Kingdom of Saudi Arabia
[h]Functional Materials Group, Gulf University for Science and Technology, Mubarak Al-Abdullah, 32093 Kuwait, Kuwait
[i]Centre of Research Impact and Outcome, Chitkara University Institute of Engineering and Technology, Chitkara University, Rajpura-140401, Punjab, India
[j]Department of Chemical Engineering, School of Mining, Metallurgy and Chemical Engineering, University of Johannesburg, P.O. Box 17011, Doornfontein 2028, South Africa
[k]Department of Civil Engineering, University Centre for Research & Development, Chandigarh University, Gharuan, Mohali, Punjab, India
[l]Sustainability Cluster, School of Advanced Engineering, UPES, Bidholi, Dehradun, Uttarakhand 248007, India
[m]Saveetha School of Engineering, Saveetha Institute of Medical and Technical Sciences, Saveetha University, Chennai, Tamil Nadu – 602105, India
[n]Department of Wood Mechanics and Technology, Faculty of Forestry, Istanbul University-Cerrahpasa, Istanbul, Turkiye. E-mail: nadiray@istanbul.edu.tr

© 2025 The Author(s). Published by the Royal Society of Chemistry

Open Access Article. Published on 13 February 2025. Downloaded on 1/20/2026 2:38:44 PM.
This article is licensed under a Creative Commons Attribution-NonCommercial 3.0 Unported Licence.

Australia, Indonesia, North Central America, and South America.[6] It's a really nourishing fruit. Among many other nutrients, it is high in calcium, vitamin C, magnesium, iron, and potassium. This fruit is really good for coding. The insecticidal action of seed extracts is constituted by their extreme toxicity.[7] The seeds from the Coimbatore village of Othakkalmandapam were undisturbed and kept in an airtight sample tube for additional research and analysis. The characterisation techniques used were DLS, XRD, UV, FTIR, and SEM. Analysis was also done on the anti-ulcer, anti-bacterial, anti-fungal, antioxidant, and phytochemical screening.

2. Methods and materials

Analytical grade calcium chloride ($CaCl_2$) with 98% purity, sodium hydroxide (NaOH), deionized water was of analytical grade from Sigma Aldrich brand. *Annona squamosa* seeds are collected through the local farm in Othakkalmandapam, Coimbatore, Tamilnadu, India.

Table 1 Initial phytochemical screening of *A. squamosa* seeds in various extracts

S. No.	Phytochemical compound	Result
1	Resins	Absent
2	Carboxylic acid	Absent
3	Tannins	Present
4	Steroids	Absent
5	Flavanoids	Present
6	Carbohydrates	Absent
7	Glycosides	Absent
8	Saponification	Present
9	Proteins	Present
10	Phenol	Absent
11	Biuret	Present
12	Saponin	Present
13	Gum	Absent
14	Flavanoglycoside	Present
15	Alkaloids	Present

2.1 Preparation of extract from AS seeds

After harvesting fresh, mature 50 grams of *Annona squamosa* (AS) seeds from a nearby farm was taken, the outer skins were peeled off and the stalks disposed of. The seeds were then properly cleaned with deionized and distilled water to get rid of any contaminants, dust, and undesired material.[8] The AS seeds were mixed with 50 ml distilled water and boiled for half an hour. This extract was then used in the production of metal oxide nanoparticles.[9]

2.2 Phytochemical screening

Phytochemical screening for crushed *Annona squamosa* seed extracts were subjected to different qualitative tests for the detection of phytochemical constituents with tests for resins, carboxylic acid, tannins, steroids, flavanoids, glycosides (Born-Trageru's Test, Proteins (Bradford Method), phenol (Ferric Chloride Test), saponin test, saponification test, gum test, alkaloids – mayer's test, biuret test, carbohydrates were performed with specific reagents and results are revealed in Table 1.

Phytochemical screening analysis of the powdered sample of *A. squamosa* seeds revealed the presence of all the constituents and few bioactive compounds. The formation of green colour precipitate indicates the presence of resins. Colour changes occur indicates the presence of carboxylic acid. Formation of red colour indicates the presence of tannins. In the upper layer formation of red colour and in the lower layer, yellow with green colour is formation indicates the presence of steroids. The formation of yellow colour indicates the presence of flavonoids. The formation of pink colour indicates the presence of glycosides. To 500 μl of plant extract, 5 ml of the Bradford reagent was added incubated at dark for 10 to 15 min. Taken the OD at 575 nm. Presence of proteins is revealed. The formation of dark green colour indicates the presence of phenol. The formation of 2 cm layer of foam indicates the presence of saponins. The formation of soap or fat indicates the positive test for saponification. White colour cloudy precipitate indicates gums & mucilage's. The formation of pink colour indicates the presence of flavanoglycoside. Appearance of white creamy precipitate indicates the presence of alkaloids. Formation of the pink

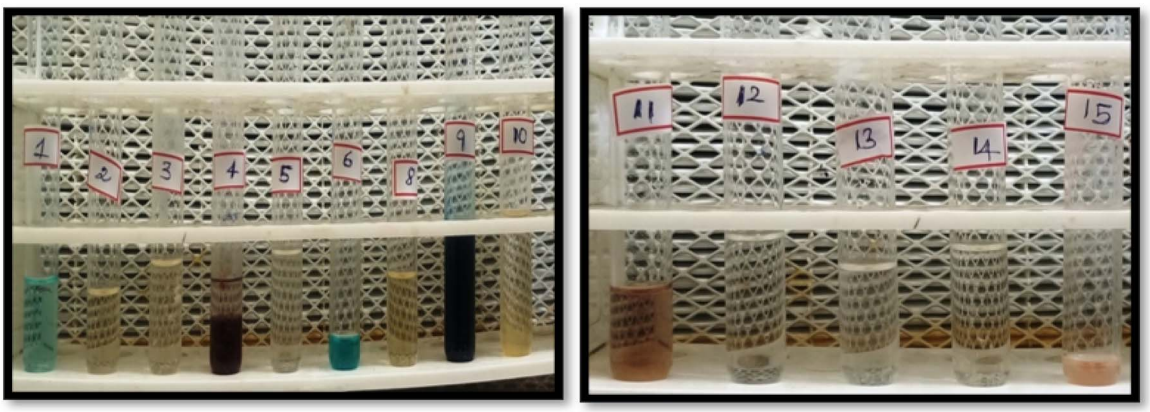

Fig. 1 Qualitative phytochemical screening methods.

Open Access Article. Published on 13 February 2025. Downloaded on 1/20/2026 2:38:44 PM.
This article is licensed under a Creative Commons Attribution-NonCommercial 3.0 Unported Licence.

colour indicates the test is positive in biuret test. Colour changes and precipitate are formed. It indicates the presence of carbohydrate is pictured in Fig. 1. Chemical examination on assorted parts of the plant has illustrated in the segregation of a large amount of novel along with interesting metabolites.[13,14]

2.3 Synthesis of calcium oxide nano particles using AS seed extracts

Calcium oxide nanoparticles were synthesized using calcium chloride and custard apple seed extract as precursors. A 1 M calcium chloride solution was created by dissolving it in deionized water. The calcium chloride and custard apple seed extract were united in a 1 : 1 ratio.[10,11] The reaction mixture was maintained at a temperature below boiling while being stirred at 800 rpm using a magnetic stirrer. After half an hour, NaOH is added dropwise to attain pH 12. After maintaining the pH value, the mixture turned reddish-brown. This process was conducted in a dark environment. Following the reaction, the suspension was centrifuged at 15 000 rpm for 15 minutes, consequential in a yellow paste (Fig. 2). This paste was then filtered through filter paper as well as placed in a crucible for heating. The precipitate was worked up in a muffle furnace at 400 °C for 3 hours to remove any moisture. The resulting precipitate, identified as AS-CaO nanoparticles,[12] is illustrated in Fig. 2. The nanoparticles were kept in a cool, dry, and dark environment for characterization and future applications.

3. Result and discussion

3.1 UV-vis absorption spectroscopy examination

Fig. 3 illustrates the absorption spectra of AS-CaO nanoparticles, highlighting a peak around 323 nm. Additionally, a peak corresponding to the AS seed extracts is observed at 310 nm, likely due to the presence of bioactive polyphenolic

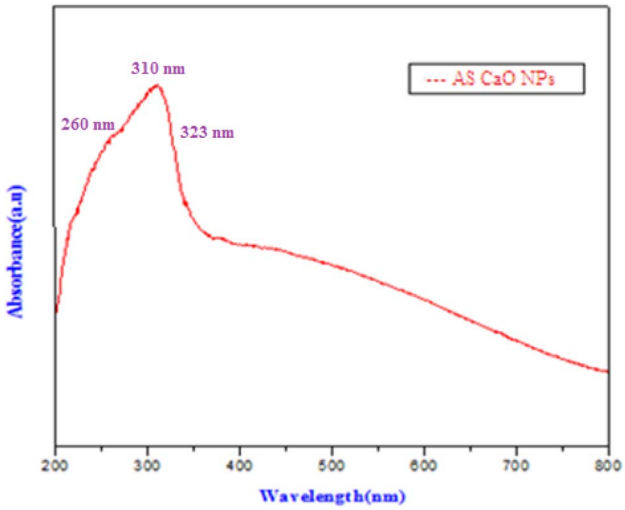

Fig. 3 UV-visible analysis of AS-CaO.

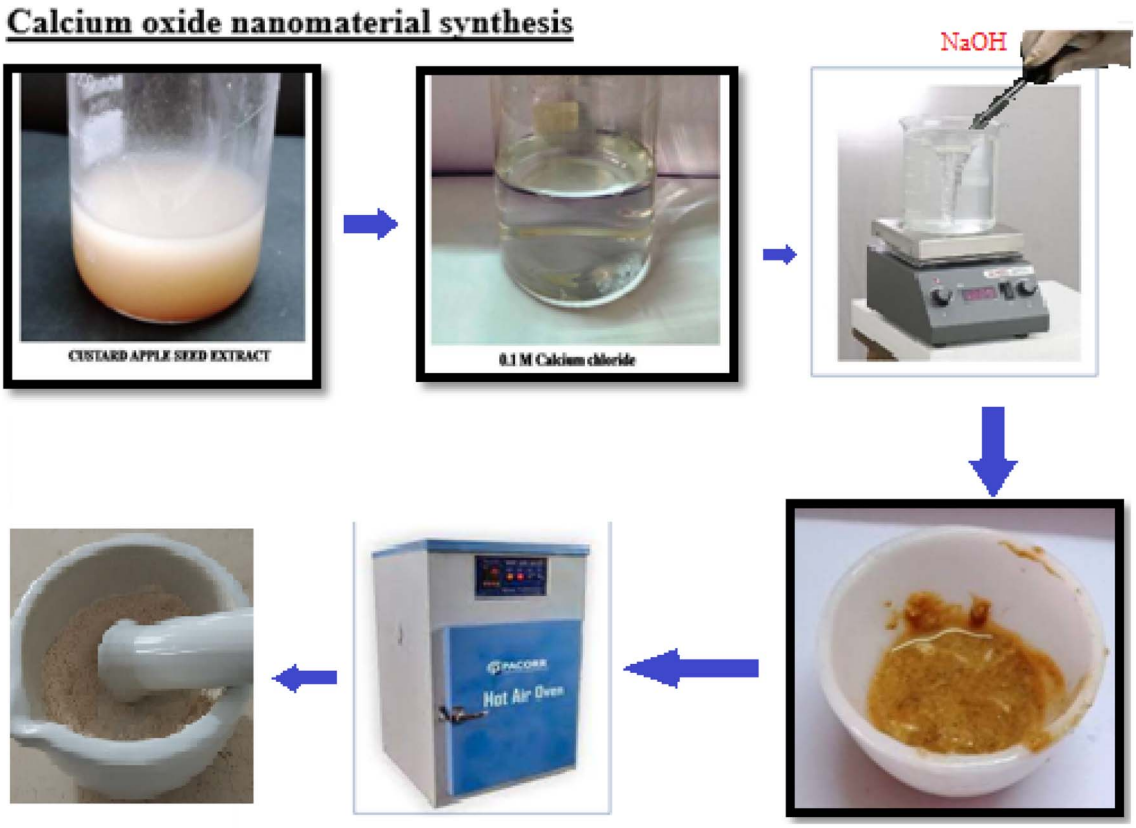

Fig. 2 CaO nanoparticle synthesis.

 © 2025 The Author(s). Published by the Royal Society of Chemistry

Open Access Article. Published on 13 February 2025. Downloaded on 1/20/2026 2:38:44 PM.
This article is licensed under a Creative Commons Attribution-NonCommercial 3.0 Unported Licence.

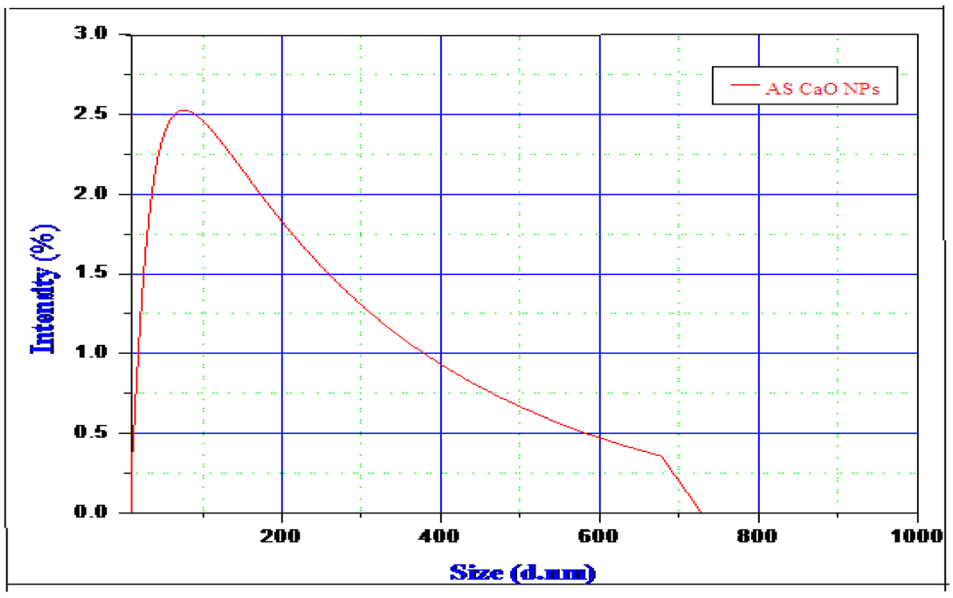

Fig. 4 DLS analysis of AS-CaO NPs.

compounds that facilitate the fall of calcium ions to CaO nanoparticles. The solid-state AS-CaO nanoparticles display exciton absorption at 310 nm in their UV-vis spectra, with a notable excitation binding energy at 25 °C. The UV-vis analysis of CaO nanoparticles clearly indicates to facilitate the nanomaterial has high absorption ability in the visible spectrum.[15,16]

3.2 DLS analysis

One practical method for modifying the size and shape of nanorods in a fluid media is the dynamic light scattering approach. The diameter of nanoparticles disseminated in fluid is terminated by the DLS. Furthermore, it establishes the distribution and size of particles in physiological fluids.[13,17] The dynamic light scattering (DLS) examination of the AS CaO NPs size distribution histogram reveals a hydrodynamic diameter of 600 nm and 700 nm, with abrupt peak in the intensity. As seen in Fig. 4, it is practical for each polymeric surfactant solution to have a single peak.[18]

Using DLS analysis, the phytosynthesized AS-CaO nanoparticles were shown to have a greater mean size of 600–700 nm and a very narrow scatter (standard deviation: 2.5%). This

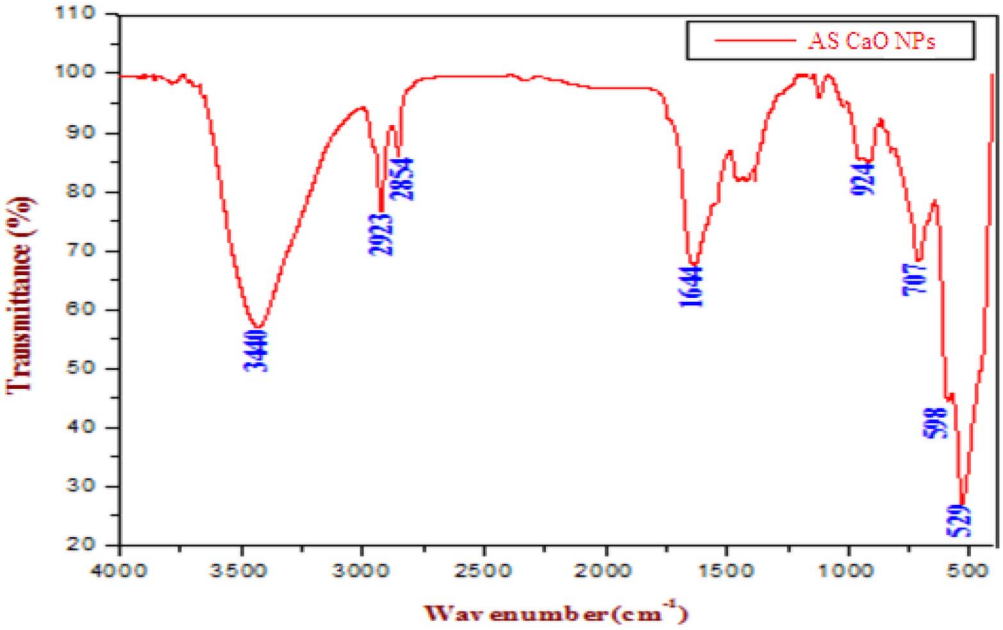

Fig. 5 Fourier transform infra-red analysis of AS-CaO.

Open Access Article. Published on 13 February 2025. Downloaded on 1/20/2026 2:38:44 PM.
This article is licensed under a Creative Commons Attribution-NonCommercial 3.0 Unported Licence.

behavior can be attributed to the two times the amount of seed extract that is available for reducing $CaCl_2$, which causes the nanoparticles to expand and nucleate more abruptly while occasionally forming tiny agglomerates.[15,19]

3.3 Fourier transform infra-red analysis

The AS-CaO nanoparticles were analyzed using infrared (IR) measurements at room temperature, employing the KBr method over a wavenumber range of 400 to 4000 cm^{-1}. A low-energy peak observed at 529 cm^{-1} indicates the bending vibration of the CaO bond.[16] In the 400–600 cm^{-1} range, Ca–oxygen interactions are predominant. The prominent peak at 3600–3450 cm^{-1} in the higher energy region corresponds to the stretching vibration of the –OH group.[20]

The –CH stretching vibration band, indicative of alkane groups, first appears around 2923 cm^{-1}. Peaks between 1620 and 1655 cm^{-1} correspond to the amide I and amide III regions found in proteins and enzymes. Notable bands in the range of 1120 to 1065 cm^{-1}, linked to C–O stretching vibrations,[17,21] suggest the presence of carboxylic acid and alcohol functional groups. The FT-IR spectra reveal absorption bands at 3440, 2923, and 1644 cm^{-1},[22] which correspond to the structure of *Annona squamosa* (AS) seeds. These peaks are influenced by high levels of phytochemical constituents, as illustrated in Fig. 5.

Thus, the bioreduction process is influenced by components that are water-soluble flavonoids and phenolic acids. AS-CaO nanoparticles can be generated through the interaction of calcium ions with reducing phenolic acids, including ascorbic acid, cardiac glycosides, and gallic acid.[23] One potential mechanism is the decrease of calcium nitrate ions, which results in create intermediate complexes with the phenolic –OH groups found in hydrolyzable tannins, resulting in their oxidation to quinone forms. This mechanism may explain how ascorbic acids from *Annona squamosa* seeds stabilize the green synthesis of CaO nanoparticles.[17,24] Further research is needed, as the exact process is not yet fully understood.

Table 2 Average crystalline size

Sample name	2θ (degree)	D spacing	FHWM	hkl value	Lattice constant	Unit cell $V = abc$	Avg. crystalline size
CaO	29.52	0.9734	0.4428	011	$a = 4.3758$	82.94	3.722505
	32.22	1.9685	0.5904	111			
	37.35	2.4056	0.492	002	$b = 4.397$		
	42.81	2.7060	0.492	012			
	53.83	3.7016	0.2952	022	$c = 4.3112$		
	64.09	3.9542	0.594	113			
	67.34	4.125	0.7872	222			

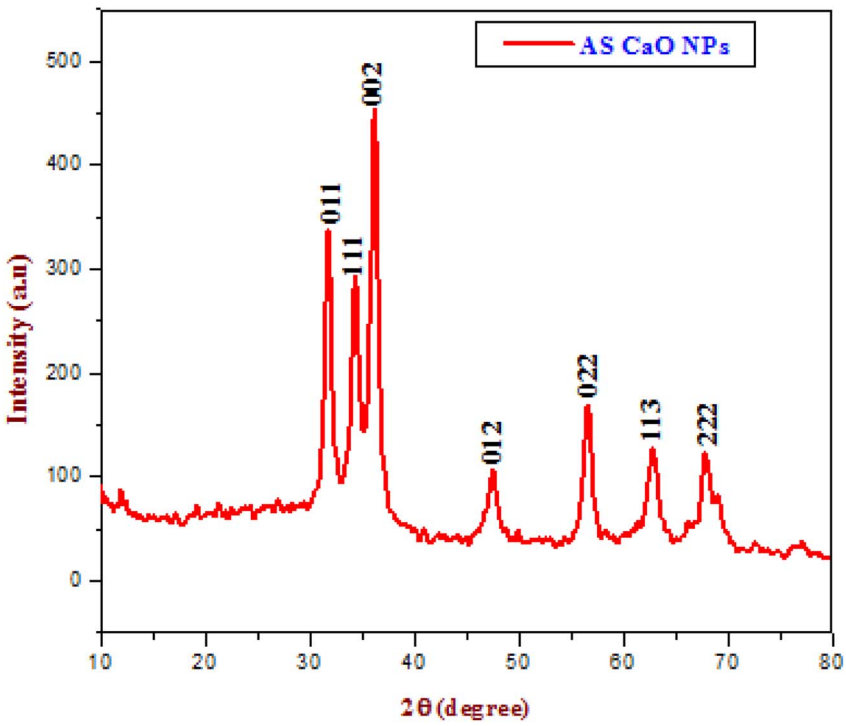

Fig. 6 X-ray diffraction pattern analysis.

 © 2025 The Author(s). Published by the Royal Society of Chemistry

Open Access Article. Published on 13 February 2025. Downloaded on 1/20/2026 2:38:44 PM.
This article is licensed under a Creative Commons Attribution-NonCommercial 3.0 Unported Licence.

3.4 X-ray diffraction analysis

CaO NPs are visible at 29.59°, 32.22°, 37.35°, 42.81°, 53.83°, 64.09°, and 67.34° in the XRD patterns. These align with the (011), (111), (002), (012), (022), (113), and (222) planes of the cubic system for CaO nanoparticles,[19] as exposed in Table 2.

The cubic crystal structure and lattice parameters (Å) of CaO (JCPDS card no. 00-078-0649) align with the observed values in the XRD patterns. The recorded peak intensities confirm the cubic structure, with Fig. 6 illustrating the notably high strength of the (002) peak, suggesting anisotropic expansion and a favoureddirection of the crystallites. The sharp and narrow diffraction peaks suggest excellent crystalline quality.[19,25] No other crystalline imperfections are evident, and the diffraction peaks remain unchanged. Calculation of *d*-spacing between calcium oxide nanoparticles. It can be calculated by using Bragg's equation

$$n_\lambda = 2d \sin\theta \tag{1}$$

Scherrer equation

$$D = \frac{K\lambda}{\beta \cos\theta} \tag{2}$$

Lattice parameters

$$\frac{1}{d^2} = \frac{h^2}{a^2} + \frac{k^2}{b^2} + \frac{l^2}{c^2} \tag{3}$$

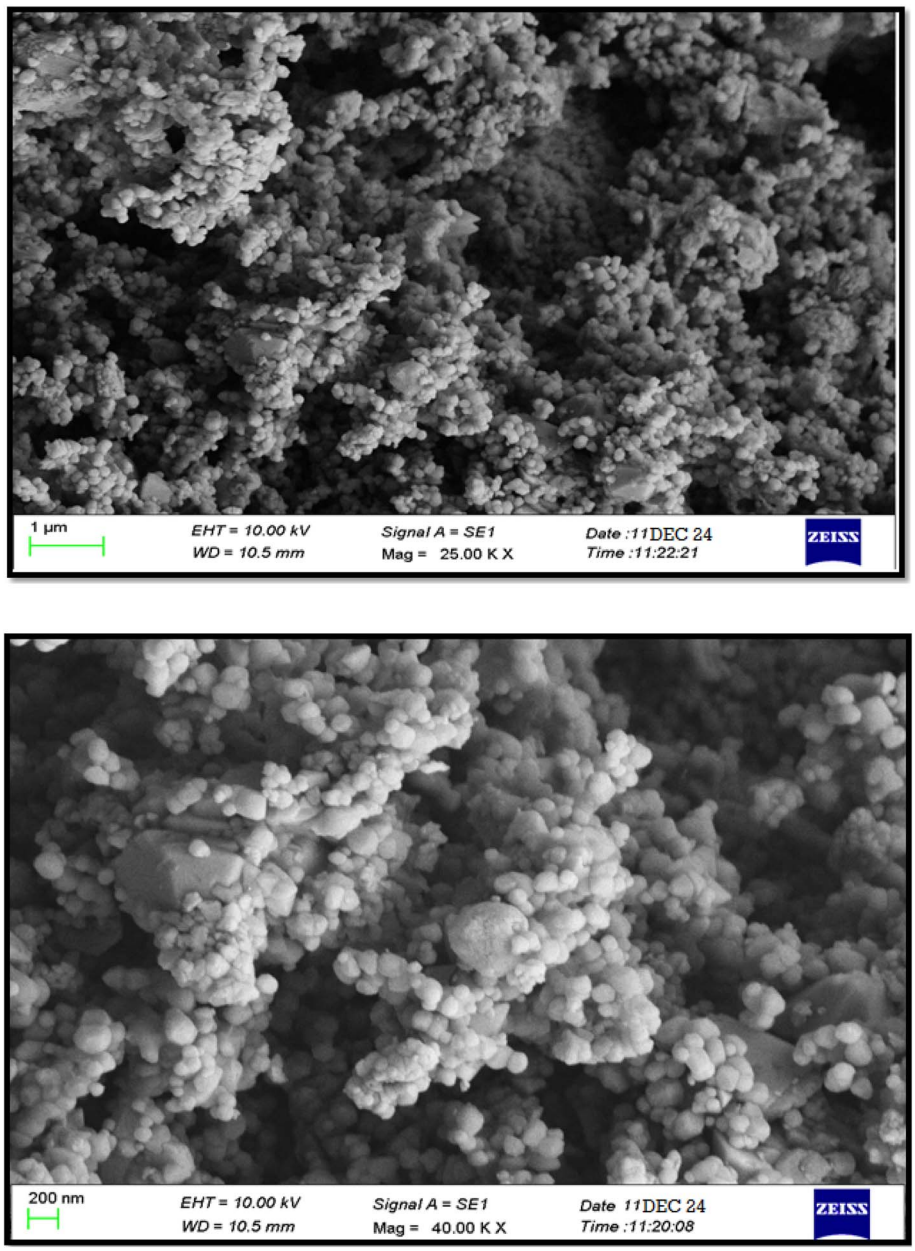

Fig. 7 FESEM images of CaO nanoparticles.

Open Access Article. Published on 13 February 2025. Downloaded on 1/20/2026 2:38:44 PM.
This article is licensed under a Creative Commons Attribution-NonCommercial 3.0 Unported Licence.

$$\text{Unit cell volume } (V) = abc\ (\text{Å})^3 \quad (4)$$

where, λ-X-ray wavelength in Å, n – diffraction order, d-distance between neighboring CaO layers. θ-diffraction angle in degree. D – mean crystallite size in Å, K (constant) shape-dependent constant for crystallites (0.9 factor), a, c – lattice parameters. By using the above equations, the lattice parameters of the prepared CaO NPs is $a = 4.3758$, $b = 4.397$, $c = 4.3112$, unit cell volume is 83.94 and mean or average particle size is 3.72 nm.

3.5 FESEM analysis

The FESEM micrograph depicts the morphology of the CaO nanoparticles, showing that they consist of spherical masses that are agglomerated and clustered together, as seen in Fig. 7. The spherical shaped CaO nanoparticles present due to influenced of the plant extract of *Annona squamosa* seed extracts. It is clearly shows in the FESEM image. Moreover, the this spherical shaped particles suggests that the standard size of the nanoparticles is under 100 nm.

Such an agglomerated and clumped structure could be explained by the *Annona squamosa* (AS) seeds' supersaturated nature.[21,26,27] Likewise, the observation that these particles are formed during the precipitation process through the fusion of smaller particles is supported by the spherical morphology and limited agglomeration of the CaO nanoparticles.[28] This discovery has demonstrated that, despite the calcium particles' varied production processes, they all share a similar form.

3.6 Antibacterial activity

Bacterial strains (*P. aeruginosa* and *P. acnes*) were cultured for 24 hours on Petri dishes including 20 milliliters of nutrient agar medium. After wells were produced in the agar, varying concentrations of Ca nanoparticles (500 μg ml^{-1}, 250 μg ml^{-1}, 100 μg ml^{-1}, and 50 μg ml^{-1}) were added. The plates were incubated for 24 hours at 37 °C. The antibacterial activity was evaluated by measuring the diameter of the inhibition zone approximately the wells. Gentamicin served as a positive control. Data investigation was conducted using GraphPad Prism 6.0 software from the USA.[29–32] The zone of inhibition was measured in triplicate, and the results are reported as mean ± standard deviation. Error bars in the figures represent the standard deviation of three independent experiments.

P. acnes 15.5 ± 0.7, had the maximum zone of growth inhibition, followed by *P. aeruginosa* 12.5 ± 0.7 for 500 μg ml^{-1}. *P. acnes* 8 ± 0.7, had the maximum zone of growth inhibition, followed by *P. aeruginosa* 7.5 ± 0.7 for 250 μg ml^{-1}. *P. acnes* 6.5 ± 0.7, had the maximum zone of growth inhibition, followed by *P. aeruginosa* 6.5 ± 0.7 for 100 μg ml^{-1}. No zone of inhibition was identified for 50 μg ml^{-1}.[33] Additionally, as compared to the control chemical Gentamicin antibiotic, produced AS CaO NPs exhibit reduced antibacterial activity, and this result was confirmed by the findings in Fig. 8, 9 and tabulated in Table 3.[50]

3.7 Anti-fungal activity

A 72 hour culture of *Aspergillusflavus* and *Aspergillusfumigatus* was inoculated into Petri plates including 20 ml of potato dextrose agar medium. Wells were then created, and a range of concentrations of Ca nanoparticles (500, 250, 100, and 50 μg ml^{-1}) were introduced. The plates were incubated for 48–72 hours at 37 °C. The diameter of the inhibition zone around the wells was measured to evaluate the antifungal activity. Amphotericin B at 100 units served as a positive control.[34–36] Data investigation was conducted using GraphPad Prism 6.0 software from the USA. The zone of inhibition was measured in triplicate, and the results are reported as mean ± standard deviation. Error bars in the figures represent the standard deviation of three independent experiments.

Aspergillusflavus 6 ± 0.7, had the maximum zone of growth inhibition, followed by *Aspergillusfumigatus* 5.5 ± 0.7 for 500 μg ml^{-1}. *P. acnes* 8 ± 0.7, had the maximum zone of growth inhibition, followed by *P. aeruginosa* 7.5 ± 0.7 for 250 μg ml^{-1}. *P. acnes* 6.5 ± 0.7, had the maximum zone of growth inhibition, followed by *P. aeruginosa* 6.5 ± 0.7 for 100 μg ml^{-1}. No Zone of inhibition was identified for 250 100 and 50 μg ml^{-1}.

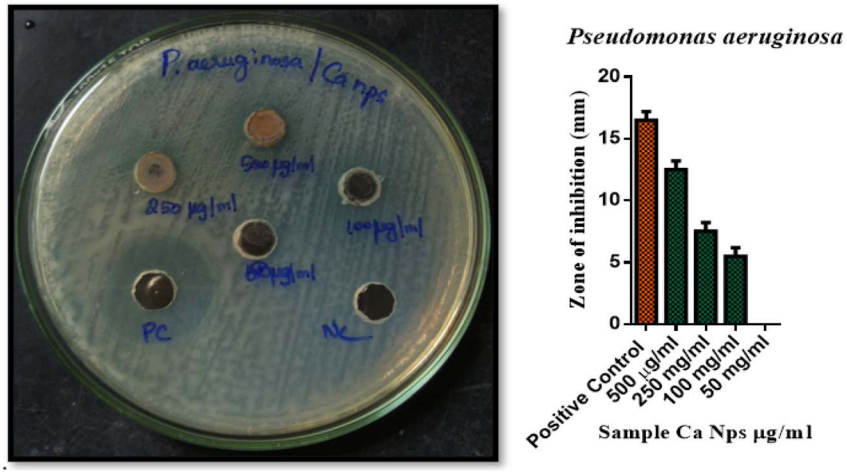

Fig. 8 Effect of sample Ca Nps against *P. aeruginosa*.

 © 2025 The Author(s). Published by the Royal Society of Chemistry

Open Access Article. Published on 13 February 2025. Downloaded on 1/20/2026 2:38:44 PM.
This article is licensed under a Creative Commons Attribution-NonCommercial 3.0 Unported Licence.

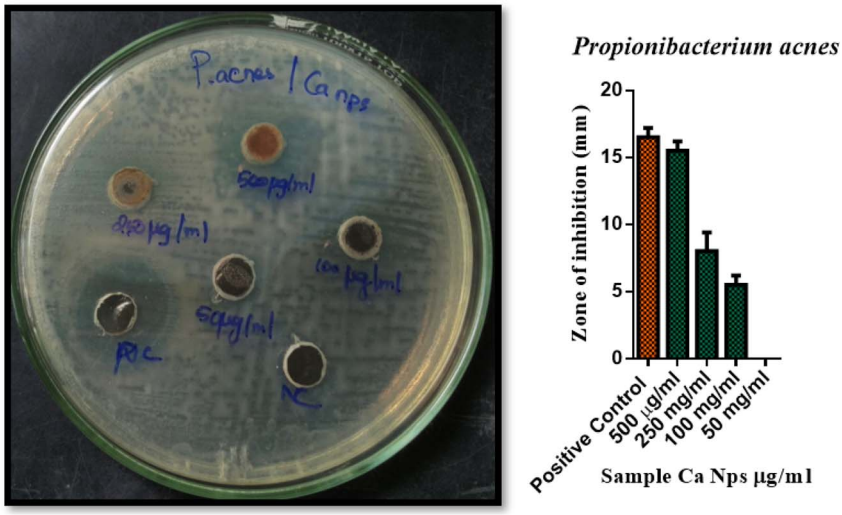

Fig. 9 Effect of sample Ca Nps against *P. acnes*.

Table 3 SD ± means of zone of inhibition obtained by sample – Ca NPs against (*P. aeruginosa and P. acnes*)

			Zone of inhibition (Mm) SD ± mean				
S. No.	Name of the organism	Name of the test sample	PC	500 µg µl^{-1}	250 µg µl^{-1}	100 µg µl^{-1}	50 µg µl^{-1}
1	*P. aeruginosa*	Sample – CaNps	16.5 ± 0.7	12.5 ± 0.7	7.5 ± 0.7	6.5 ± 0.7	0
2	*P. acnes*		16.5 ± 0.7	15.5 ± 0.7	8 ± 0.7	6.5 ± 0.7	0

Additionally, as compared to the control chemical amphotericin B (100 units), produced AS CaO NPs exhibit reduced antibacterial activity,[37,38] and this result was confirmed by the findings through Fig. 10, 11 and datas are tabulated in Table 4.

3.8. Anti-ulcer activity

3.8.1. Acid neutralizing capacity. The acid-neutralizing ability of Ca nanoparticle extracts at various concentrations (500, 250, 100, 50, and 10 µg ml^{-1}) was compared to a standard antacid composed of magnesium hydroxide and aluminum hydroxide (50 mg ml^{-1}). Once the mixture reached the 5 ml mark, water was added to get the total volume to 70 ml.[39,40] The combination was then stirred for one minute. Subsequently, 30 milliliters of 1.0 N HCl was added to both the standard and test mixtures, which were mixed for 15 minutes. Afterward, drops of phenolphthalein solution were introduced and diverse in. The overload HCl was titrated with 0.5 N sodium hydroxide solution, drop by drop, until a pink color was achieved. The outcomes are tabulated in Table 5.[37,41]

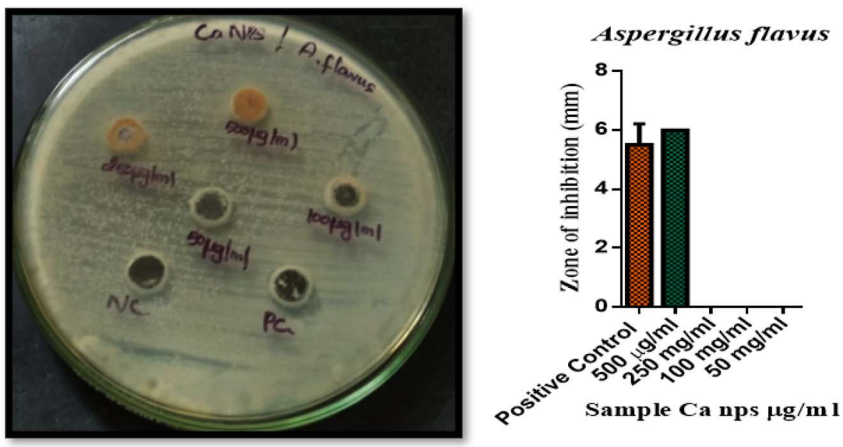

Fig. 10 Effect of sample Ca NPs against *Aspergillusflavus*.

Open Access Article. Published on 13 February 2025. Downloaded on 1/20/2026 2:38:44 PM.
This article is licensed under a Creative Commons Attribution-NonCommercial 3.0 Unported Licence.

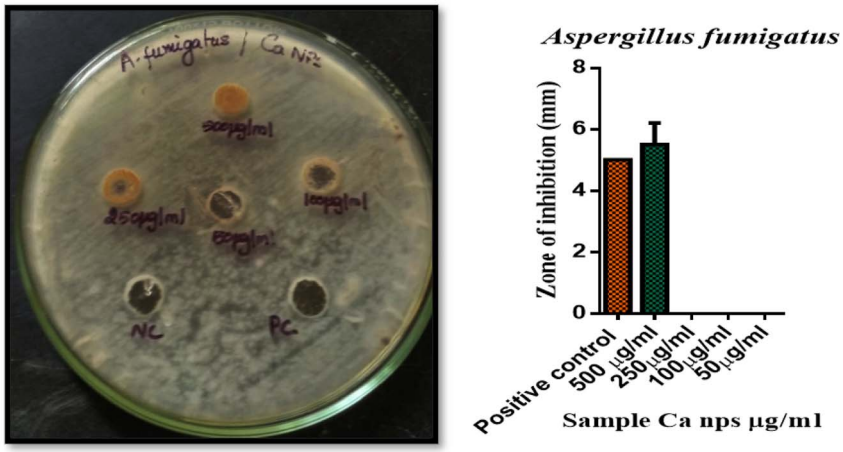

Fig. 11 Effect of sample Ca NPs against *Aspergillusfumigatus*

Table 4 SD ± means of zone of inhibition obtained by sample Ca NPs against *Aspergillusflavus* and *Aspergillusfumigatus*

			Zone of inhibition (mm) SD ± mean				
S.·No.	Name of the organism	Name of the test sample	PC	500 μg μl^{-1}	250 μg μl^{-1}	100 μg μl^{-1}	50 μg μl^{-1}
1	*A. flavus*	Ca NPs	5.5 ± 0.7	6 ± 0.7	0	0	0
2	*A. flumigatus*		5 ± 0	5.5 ± 0.7	0	0	0

Table 5 Moles of acid neutralized

S. No.	Name of the sample	Reading a burette in cm	Moles of acid neutralized	Acid neutralizing capacity (ANC)/antacid (g)
1	Control	2.5	1.75	35
2	500 μg ml^{-1}	1.5	2.5	45
3	250 μg ml^{-1}	1.8	2.1	42
4	100 μg ml^{-1}	2	2	40
5	50 μg ml^{-1}	2.3	1.85	37
6	10 μg ml^{-1}	2.5	1.75	35

The number of moles of acid neutralized is calculated by:

$$\text{Moles of acid neutralized} = (\text{vol. of HCl} \times \text{normality of HCl}) - (\text{vol. of NaOH} \times \text{normality of NaOH})$$

$$\text{Acid neutralizing capacity per gram of antacid (ANC)} = \frac{\text{moles of HCl neutralized}}{\text{grams of antacid/extract}}$$

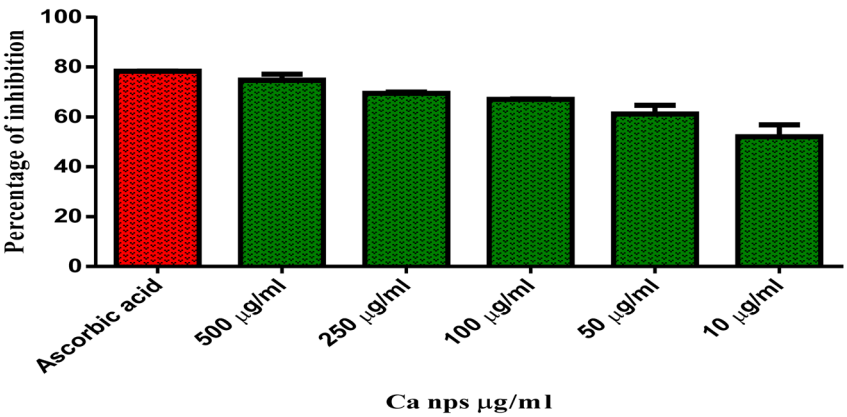

Fig. 12 Moles of acid neutralized.

 © 2025 The Author(s). Published by the Royal Society of Chemistry

Open Access Article. Published on 13 February 2025. Downloaded on 1/20/2026 2:38:44 PM.
This article is licensed under a Creative Commons Attribution-NonCommercial 3.0 Unported Licence.

Table 6 Percentage of inhibition

S. No.	Concentration of the tested sample ($\mu g\ ml^{-1}$)	Inhibition percentage (in triplicates)			Average value (%)
1	$Asco_4$rbic acid	78.42	78.27	78.27	78.34
2	500 $\mu g\ ml^{-1}$	77.29	74.43	72.48	74.88
3	250 $\mu g\ ml^{-1}$	70.07	69.32	69.32	69.69
4	100 $\mu g\ ml^{-1}$	66.91	67.21	67.21	67.06
5	50 $\mu g\ ml^{-1}$	57.14	63.23	63.23	60.18
6	10 $\mu g\ ml^{-1}$	57.59	49.24	49.24	53.42

3.9. Anti-oxidant activity

At lower concentrations, the bio-mediated calcium oxide nanoparticles were less successful at scavenging free radicals; nevertheless, at higher concentrations, they demonstrated remarkable efficacy, on par with normal ascorbic acid. The results of the experiment revealed that free essential scavenging is a concentration-dependent process that is also impacted by the prepared samples' dimensions.[42–45] The phytoconstituents in the specific extracts may be responsible for the enhanced capacity of metal nanoparticles to scavenge free radicals.[46–49] Fig. 12 shows the percentage of inhibition, while Table 6 records the values.

4. Conclusion

The current study examined the antibacterial, antioxidant, and antiulcer properties of CaO nanoparticles produced by a green manufacturing method. Nanoparticles with regulated sizes and morphologies are produced by synthesis using plant extract. Studies using XRD and FESEM verified the creation of spherically-shaped nano CaO with 37 nm crystallite size. When tested against the indicated bacterial pathogens, antibacterial activities showed good activity. We conclude that the environmentally friendly manufacture of calcium oxide nanoparticles is a simple as well as rational procedure capable of yielding extremely stable metallic nanoparticles. Greenly manufactured nanoparticles have very little cytotoxicity and are not harmful to erythrocytes. These nanoparticles have strong antioxidant and antibacterial properties. The production of flavonoids and phenolics increased stability, allowing CaO NPs to be used *in vivo*. Further stabilization techniques along with a variety of manufacturing methods for calcium oxide nanoparticles can overlay the road for their potential medical uses.

Data availability

Data will be made available on request.

Author contributions

Sarathamani T, and Kalaiselvi V conducted a literature search and drafted the manuscript; Gopi S, and Blessymol B conceived the idea and recommended a structure for this research; Khatib Sayeed Ismail, Syed Kashif Ali, designed and created the figures and finished tables. Gulrana Khuwaja, Sivasubramanian Palanismy, Mika Sillanpaa and Nadir Ayrilmis helped to edit and revise the manuscript. All the authors listed have read and approved the final manuscript.

Conflicts of interest

The authors have declared no conflict of interest.

References

1 D. S. Goodsell, *Bionanotechnology: Lessons from Nature*, John Wiley & Sons, 2004.
2 W. C. W. Chan and S. Nie, *Science*, 1998, **281**, 2016–2018.
3 P. Kumbhakar, A. Pramanik, S. Biswas, A. K. Kole, R. Sarkar, C. S. Tiwary and P. Kumbhakar, in *Photocatalytic Degradation of Dyes*, Elsevier, 2021, pp. 167–206.
4 D.-H. Bae, J.-H. Yeon, S.-Y. Park, D.-H. Lee and S.-D. Ha, *Arch. Pharmacal Res.*, 2006, **29**, 298–301.
5 N. Gandhi, Y. Shruthi, G. Sirisha and C. R. Anusha, *Saudi J. Life Sci.*, 2021, **6**, 89–103.
6 S. V. Rabelo, J. de S. S. Quintans, E. V. Costa, J. R. G. da Silva Almeida and L. J. Q. Júnior, *Essential Oils in Food Preservation, Flavor and Safety*, 2016, pp. 221–229.
7 T. Handayani, in *IOP Conference Series: Earth and Environmental Science*, IOP Publishing, 2021, vol. 914, pp. 12062.
8 M. A. Y. Abdualrahman, H. Ma, C. Zhou, A. E. A. Yagoub, A. O. Ali, H. E. Tahir and A. Wali, *Arabian J. Chem.*, 2019, **12**, 4514–4521.
9 N. Madhusudhana, K. Yogendra and K. M. Mahadevan, *Int. J. Eng. Res. Ind. Appl.*, 2012, **2**, 1300–1307.
10 V. P. Aswathi, S. Meera, C. G. A. Maria and M. Nidhin, *Nanotechnol. Environ. Eng.*, 2023, **8**, 377–397.
11 G. Khaliq, M. Ullah, S. A. Memon, A. Ali and M. Rashid, *J. Food Meas. Char.*, 2021, **15**, 707–716.
12 F. Jamil, M. Al-Riyami, L. Al-Haj, A. H. Al-Muhtaseb, M. T. Z. Myint, M. Baawain and M. Al-Abri, *Int. J. Energy Res.*, 2021, **45**, 17189–17202.
13 A. Roy, S. S. Gauri, M. Bhattacharya and J. Bhattacharya, *J. Biomed. Nanotechnol.*, 2013, **9**, 1570–1578.
14 S. Lakshmi and G. S. Dhanya, *Int. Res. J. Pharm. Appl. Sci.*, 2013, **3**, 29–31.
15 P. Chen, Y. Wang, S. He, P. Wang, Y. Xu and L. Zhang, *Adv. Mater. Sci. Eng.*, 2020, **2020**, 9501897.

Open Access Article. Published on 13 February 2025. Downloaded on 1/20/2026 2:38:44 PM.
This article is licensed under a Creative Commons Attribution-NonCommercial 3.0 Unported Licence.

16 H.-X. Bai, X.-Z. Shen, X.-H. Liu and S.-Y. Liu, *Trans. Nonferrous Met. Soc. China*, 2009, **19**, s674–s677.
17 S. Abraham and V. P. Sarathy, *Int. J. Pharm. Sci. Rev. Res.*, 2018, **49**, 121.
18 M. Harshitha, R. D'souza, S. D. Akshay, A. Nayak, S. Disha, V. Aditya, U. S. Akshath, S. Dubey, H. M. Munang'andu and A. Chakraborty, *World J. Microbiol. Biotechnol.*, 2024, **40**, 250.
19 A. Anantharaman, S. Ramalakshmi and M. George, *Int. J. Eng. Res. Ind. Appl.*, 2016, **6**, 27–31.
20 S. Hernández Anzaldo, U. Arroyo Abad, A. León García, D. Ramírez Rosales, R. Zamorano Ulloa and Y. Reyes Ortega, *Molecules*, 2016, **21**, 804.
21 B. Adebayo-Tayo, A. Salaam and A. Ajibade, *Heliyon*, 2019, **5**(10), e02502.
22 R. G. Bodade, R. Kumar and R. Kutty, in *Nanoparticles in Green Organic Synthesis*, Elsevier, 2023, pp. 351–399.
23 E. Valanciene, I. Jonuskiene, M. Syrpas, E. Augustiniene, P. Matulis, A. Simonavicius and N. Malys, *Biomolecules*, 2020, **10**, 874.
24 R. Eram, P. Kumari, P. K. Panda, S. Singh, B. Sarkar, M. A. Mallick and S. K. Verma, *J. Nanotheranostics.*, 2021, **2**, 51–62.
25 E. Arul, K. Raja, S. Krishnan, K. Sivaji and S. J. Das, *J. Nanosci. Nanotechnol.*, 2018, **18**, 5790–5793.
26 S. S. Tabrizi Hafez Moghaddas, S. Samareh Moosavi and R. Kazemi Oskuee, *Biomass Convers. Biorefin.*, 2024, **14**, 5125–5134.
27 N. Kumaresan, K. Ramamurthi, S. Mathuri, M. M. A. Sinthiya, T. Manimozhi, M. M. Margoni and R. Rameshbabu, *Int. J. ChemTech Res.*, 2015, **7**, 1598–1602.
28 A. Rezaei, E. Katoueizadeh and S. M. Zebarjad, *Mater. Today Chem.*, 2022, **26**, 101239.
29 L. B. de Menezes, P. C. L. Muraro, D. M. Druzian, Y. P. M. Ruiz, A. Galembeck, G. Pavoski, D. C. R. Espinosa and W. L. da Silva, *J. Photochem. Photobiol., A*, 2024, **447**, 115182.
30 Y. Mbenga, M. S. Mthana, D. M. N. Mthiyane, O. E. Ogunjinmi, M. Singh and D. C. Onwudiwe, *Inorg. Chem. Commun.*, 2023, **151**, 110581.
31 K. Gebremedhn, M. H. Kahsay and M. Aklilu, *J. Pharm. Pharmacol.*, 2019, **7**, 2150–2328.
32 V. Ponnarasan and A. Krishnan, *Int. J. Nanosci.*, 2017, **16**, 1650031.
33 A. E. Al-Snai, *IOSR J. Pharm.*, 2019, **9**, 22–103.
34 S. Vijayakumar, M. Divya, B. Vaseeharan, S. Ranjan, V. Kalaiselvi, N. Dasgupta, J. Chen and E. F. Durán-Lara, *J. Cluster Sci.*, 2021, **32**, 983–993.
35 V. Ramya, V. Kalaiselvi, S. K. Kannan, M. Shkir, H. A. Ghramh, Z. Ahmad, P. Nithiya and N. Vidhya, *Arabian J. Sci. Eng.*, 2022, **47**, 909–918.
36 S. Naz, A. Gul, M. Zia and R. Javed, *Appl. Microbiol. Biotechnol.*, 2023, **107**, 1039–1061.
37 A. A. Radhakrishnan and B. B. Beena, *Indian J. Adv. Chem. Sci.*, 2014, **2**, 158–161.
38 Z. Alhalili, *Arabian J. Chem.*, 2022, **15**, 103739.
39 F. Anjum, M. Shaban, M. Ismail, S. Gul, E. M. Bakhsh, M. A. Khan, U. Sharafat, S. B. Khan and M. I. Khan, *ACS Omega*, 2023, **8**, 17667–17681.
40 M. Ahamed, H. A. Alhadlaq, M. A. M. Khan, P. Karuppiah and N. A. Al-Dhabi, *J. Nanomater.*, 2014, **2014**, 637858.
41 A. Manjunath, M. Irfan, K. P. Anushree, K. M. Vinutha and N. Yamunarani, *Adv. Mater. Phys. Chem.*, 2016, **6**, 263–273.
42 E. Arulkumar, S. Thanikaikarasan, T. Ahamad and S. M. Alshehri, *J. New Mater. Electrochem. Syst.*, 2023, **26**, 120–123.
43 K. Sahithya, A. K. Ekanayake, D. Hemanathan, R. Sindhu and B. Jaswanth, *Nano Biomed. Eng.*, 2024, **16**(2), 264.
44 H. T. Berede, D. M. Andoshe, N. S. Gultom, D.-H. Kuo, X. Chen, H. Abdullah, T. H. Wondimu, Y. Wu and O. A. Zelekew, *Sci. Rep.*, 2024, **14**, 2314.
45 M. J. Sadiq, *J. Photochem.*, 2018, **4**(2), 18–26.
46 S. J. Davarpanah, R. Karimian and F. Piri, *J. Appl. Biotechnol. Rep.*, 2015, **2**, 207–209.
47 L.-B. Shi, P.-F. Tang, W. Zhang, Y.-P. Zhao, L.-C. Zhang and H. Zhang, *Trop. J. Pharm. Res.*, 2017, **16**, 185–192.
48 S. M. Botsa, D. Ramadevi and K. Basavaiah, *J. Nanosci. Technol.*, 2018, 467–470.
49 B. Blessymol, P. Yasotha, V. Kalaiselvi and S. Gopi, *Results Chem.*, 2024, **7**, 101291.
50 M. Vincent, V. Sai Avvaru, M. astillo Rodríguez, M. Haranczyk and V. Etacheri, *J. Power Sources*, 2021, **506**, 230118.

 © 2025 The Author(s). Published by the Royal Society of Chemistry